Journal of Diabetes Science and Technology
Volume 7, Issue 1, January 2013
© Diabetes Technology Society

SYMPOSIUM

Single-Walled Carbon Nanotube-Based Near-Infrared Optical Glucose Sensors toward *In Vivo* Continuous Glucose Monitoring

Kyungsuk Yum, Ph.D., Thomas P. McNicholas, Ph.D., Bin Mu, Ph.D., and Michael S. Strano, Ph.D.

Abstract

This article reviews research efforts on developing single-walled carbon nanotube (SWNT)-based near-infrared (NIR) optical glucose sensors toward long-term *in vivo* continuous glucose monitoring (CGM). We first discuss the unique optical properties of SWNTs and compare SWNTs with traditional organic and nanoparticle fluorophores regarding *in vivo* glucose-sensing applications. We then present our development of SWNT-based glucose sensors that use glucose-binding proteins and boronic acids as a high-affinity molecular receptor for glucose and transduce binding events on the receptors to modulate SWNT fluorescence. Finally, we discuss opportunities and challenges in translating the emerging technology of SWNT-based NIR optical glucose sensors into *in vivo* CGM for practical clinical use.

J Diabetes Sci Technol 2013;7(1):72–87

Introduction

Diabetes affects 346 million people worldwide.[1,2] Frequent hyperglycemia can cause serious complications, including heart disease, stroke, blindness, nervous system disease, and kidney disease.[3–6] In order to avoid such complications, diabetes patients rely on glucose sensors to maintain target blood glucose levels.[7] As a consequence, effective management of diabetes requires continuous monitoring of blood glucose levels.[8] An easy-to-use and accurate continuous glucose monitoring (CGM) sensor would thus improve the quality of patients' lives and help prevent and/or reduce complications that may arise from diabetes.[5,6,8–10] The next generation of glucose sensor technology therefore focuses on *in vivo* CGM.[8,10–18]

The current standard for *in vivo* CGM is the electrochemical method that uses enzymatic reactions.[8,10,19,20] Several CGM electrochemical glucose sensors have been approved by the Food and Drug Administration and are commercially available.[2,8,21] However, these sensors still have several limitations:[8,10,16,22] they have a short lifetime (2–7 days *in vivo*), they require frequent recalibration (typically at least once a day), they use a needle-like transdermal electrode and

Author Affiliation: Department of Chemical Engineering, Massachusetts Institute of Technology, Cambridge, Massachusetts

Abbreviations: (BA) boronic acid, (CGM) continuous glucose monitoring, (CPBA) carboxyphenylboronic acid, (DX) dexamethasone, (ICG) indocyanine green, (GBP) glucose-binding protein, (MWNT) multiwalled carbon nanotube, (NIR) near-infrared, (PPEG8) polyethylene glycol, eight-member, branched polymer, (PVA) polyvinyl alcohol, (SC) sodium cholate, (SWNT) single-walled carbon nanotube, (VEGF) vascular endothelial growth factor

Keywords: continuous glucose monitoring, glucose, near-infrared fluorescence, single-walled carbon nanotube

Corresponding Author: Michael S. Strano, Ph.D., Department of Chemical Engineering, Massachusetts Institute of Technology, 77 Massachusetts Ave., Cambridge, MA 02139; email address strano@mit.edu

thus leave an open wound, they often overestimate hypoglycemia [which can limit their use with a "closed-loop" insulin pump (i.e., artificial pancreas)], and they are intrinsically susceptible to biofouling because they measure the flux of glucose rather than the concentration.

Because of their advantages over electrochemical sensors for *in vivo* continuous monitoring, noninvasive or minimally invasive optical glucose sensors are of great interest.[16,23,24] A key advantage is that optical glucose sensors do not require an electrode that physically penetrates the skin as in commercial electrochemical CGM sensors; rather these implanted sensors can be optically interrogated into the skin. Optical glucose sensors include minimally invasive, implantable fluorescence- or surface-plasmon-resonance-based sensors and completely noninvasive spectroscopic sensors.[16,23–25] Fluorescence-based sensors typically use glucose-responsive fluorophores and fluorescence resonance transfer pairs of fluorophores that emit fluorescence at visible wavelengths. However, such fluorophores often photobleach, which is intrinsically unfavorable for long-term *in vivo* glucose sensing; furthermore, fluorescence at visible wavelengths does not penetrate well through the optically turbid biological tissue.[16,23,26] On the other hand, current noninvasive spectroscopic-based sensors lack specificity and dynamic range for glucose detection.[11,12,21,24,25] For example, a noninvasive CGM sensor based on a multisensor concept, embedding dielectric spectroscopy and optical sensors, and a mathematical model is only valid for real-time monitoring of glycemic variation.[24]

Single-walled carbon nanotubes (SWNTs) have unique physical and chemical properties for applications in life sciences and medicine, including *in vivo* sensing and imaging.[27,28] Particularly, nonphotobleaching, near-infrared (NIR) fluorescence of SWNTs, and the capability to modulate SWNT fluorescence selectively in response to specific analytes offer great opportunities to develop NIR optical biomedical sensors. For example, we and others have demonstrated the selective modulation of SWNT fluorescence in response to target analytes, including glucose,[29–32] and have developed various SWNT-based NIR optical sensors,[29–37] which even operate at the single-molecule level.[38–40] Here we review research efforts on developing completely passive, implantable SWNT-based NIR optical sensors toward long-term *in vivo* CGM. We first describe the unique optical properties of SWNTs and compare SWNTs with traditional organic and nanoparticle fluorophores regarding *in vivo* optical glucose sensing. We then present our development of SWNT-based glucose sensors that use glucose-binding proteins (GBPs) and boronic acids (BAs) as high-affinity molecular receptor for glucose. Finally, we discuss challenges and opportunities in translating the emerging technology of SWNT-based NIR optical glucose sensing into *in vivo* CGM for practical clinical use.

Optical Properties of Single-Walled Carbon Nanotubes for *In Vivo* Sensing

Carbon nanotubes are a high-aspect ratio nanostructure, conceptually constructed by rolling graphene sheets into a seamless cylinder. Single-walled carbon nanotubes consist of a single layer of graphene whereas multiwalled carbon nanotubes (MWNTs) consist of multiple layers of graphene. The quasi-one-dimensionality of SWNTs imparts sharp electronic state densities at Van Hove singularities (**Figure 1**).[41] This electronic structure renders unique optical properties of SWNTs. Single-walled carbon nanotubes absorb light at photon energy E_{22} and emit fluorescence at E_{11} in the NIR wavelength range (900 to 1600 nm; **Figure 1A**).[41–43] The values of E_{11} and E_{22} depend on the chiral structure of SWNTs, denoted by the chiral index (n, m) that indicates the direction in which a graphene sheet is rolled into a cylinder; accordingly, the fluorescence properties of SWNTs vary with nanotube chiral structures (**Figure 1B**).[41,42] All atoms of SWNTs are surface atoms, sensitive to surface adsorption events.

Conventional fluorophores, including fluorescent quantum dots, typically emit fluorescence at visible wavelengths and often photobleach rapidly, whereas SWNTs emit fluorescence at NIR wavelengths (900 to 1600 nm), within the so-called biological "tissue transparency window," in which biological tissues are optically transparent (**Figure 2A**). SWNT-based sensors could thus outperform conventional visible wavelength fluorophores for applications in biological tissues, because the tissues are strongly absorbing and autofluorescent at visible wavelengths. Additionally, SWNT-based sensors could persist indefinitely, because SWNTs are nonphotobleaching (**Figure 2B**).

Next we compare the quantum yield, optical tissue transparency, tissue penetration depth, and photostability of SWNTs with those of conventional organic and nanoparticle fluorescence probes, regarding *in vivo* sensing applications.

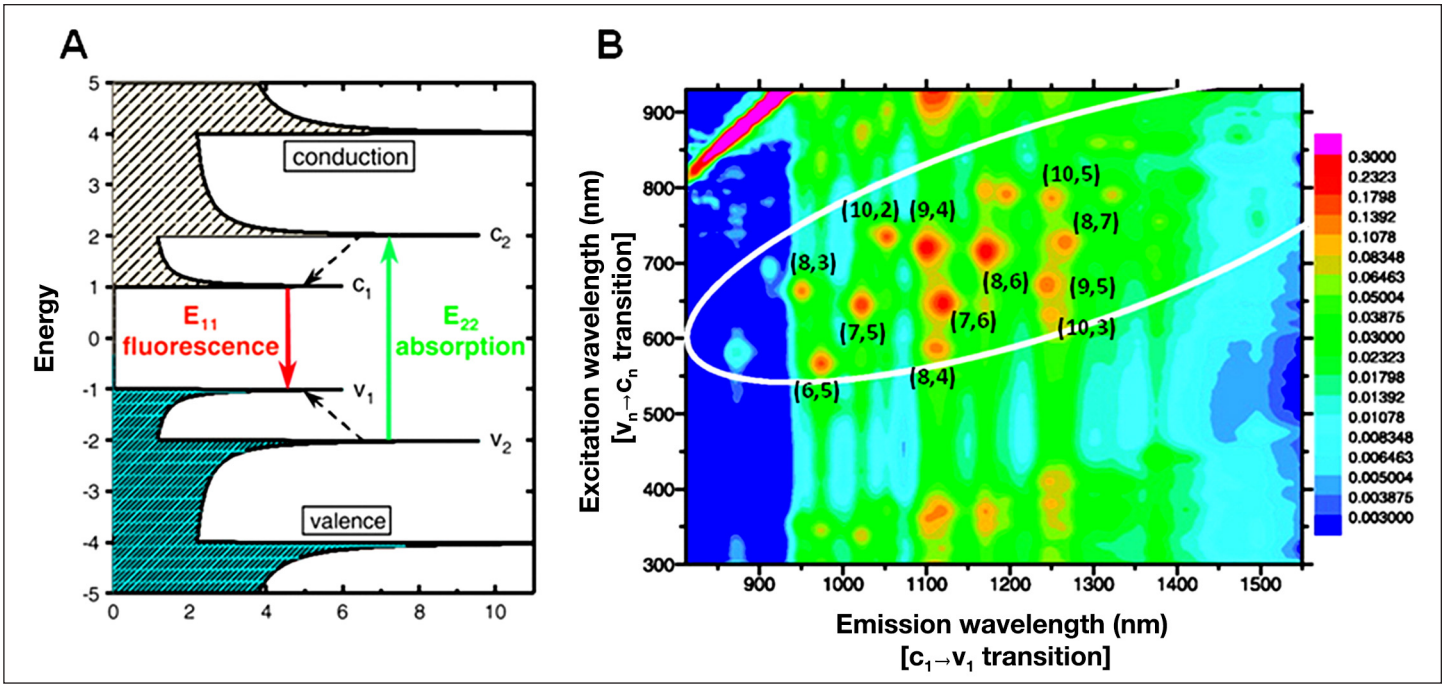

Figure 1. Optical properties of SWNTs. **(A)** Schematic density of electronic states of SWNTs. Solid arrows indicate the optical excitation and emission transitions; dashed arrows depict nonradiative relaxation of the electron in the conduction band and hole in the valence band before emission. **(B)** Fluorescence excitation–emission profile map for SWNTs. Reprinted with permission from *Science*.[41]

The intensity of the signal emitted by optical sensors is an important design constraint. For *in vivo* optical sensing, the optical signal emitted by optical sensors depends both on the quantum yield and the absorption in tissues. The quantum yield is the efficiency of energy transfer from incident light to emitted fluorescence. The absorption in biological tissues strongly depends on the wavelength (**Figure 2A**).[26] A simple one-dimensional fluorescence and absorption model estimates the fluorescent signal intensity I_S from a sensor implanted in the tissue as $I_S = I_0\phi e^{-2\mu d - k\tau}$, where I_0 is the incident excitation intensity, φ is the quantum yield, μ is the absorption coefficient, d is the distance from the surface of the tissue to the sensor implanted in the tissue, k is the pseudo-first-order photobleaching rate constant,

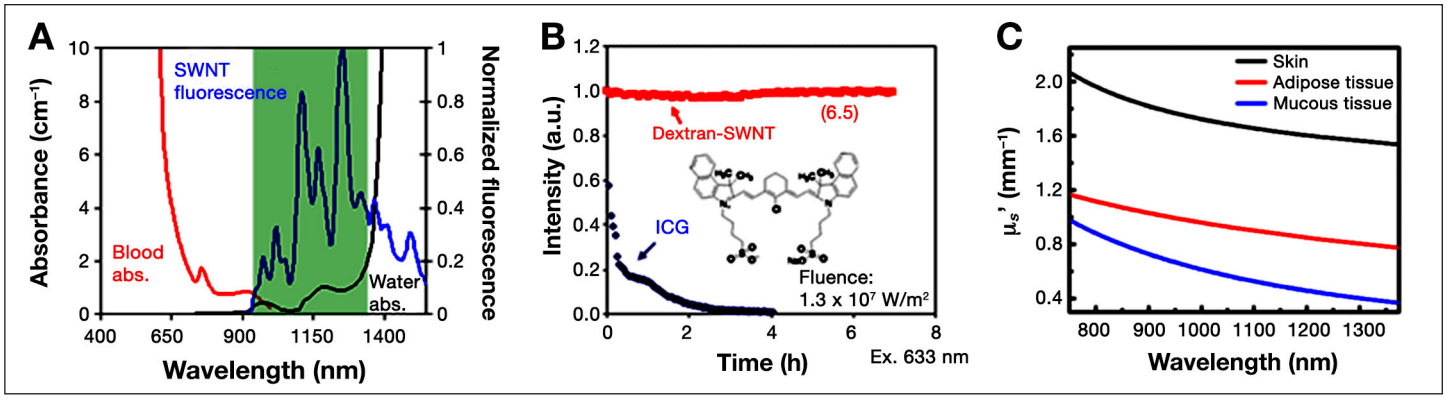

Figure 2. Fluorescence properties of SWNTs and absorption and scattering in biological tissues. **(A)** Fluorescence of SWNTs in the NIR II region. Blood (red) and water (water) absorption are significant in the visible and infrared region. The tissue transparency window, in which the tissue is optically transparent, lies between the water and blood absorption wavelength ranges. The figure includes data from Reference 26. **(B)** The fluorescence of SWNTs (red) is photostable even under high fluence (1.3×10^7 Wm^{-2}). Indocyanine green (ICG) and most organic fluorophores show a rapid photobleaching upon continuous excitation (blue). **(C)** Reduced scattering coefficient μ_s' for skin, adipose tissue, and mucous tissue as derived in Bashkatov and coauthors.[45] Scattering in the tissues decreases with increasing wavelengths: $\mu_s' \sim \lambda^{-w}$, where w depends on the size and concentration of scatters and thus varies with tissue types from 0.22 to 1.68. Reprinted with permission from *ChemSusChem*[28] and from *Proceedings of the National Academy of Sciences*.[44] Abs, absorption.

and τ is the excitation exposure lifetime.[22] **Table 1** compares the calculated value of $\phi e^{-2\mu d}$ for common organic and nanoparticle fluorophores and SWNT, which accounts for the effect of the absorption ($e^{-2\mu d}$) in I_S and determines the maximum signal emitted by an implanted sensor.[22] Despite the high quantum yield of visible fluorophores, the high absorption by tissues at visible wavelengths significantly attenuates the fluorescence signal of visible fluorophores. Moreover, low autofluorescence of tissues at NIR wavelengths renders NIR fluorophores beneficial for *in vivo* sensing applications.

Table 1.
Quantum Yield, Absorbance in Human Whole Blood (μ), and $\phi e^{-2\mu d}$ of Common Visible and Near-Infrared Organic and Nanoparticle Fluorescent Probes[a]

Fluorescent probes	Quantum yield (%)	Conditions for quantum yield measurement	Excitation (nm)	μ (oxygenated)	μ (deoxygenated)	$\phi e^{-2\mu d}$[b]
Cy5	27	PBS	620	2	60	3.20×10^{-28}
Fluorescein	95	0.1 M NaOH	496	150	120	5.23×10^{-118}
Rhodamine 6G	95	Water	488	200	105	3.30×10^{-133}
Rhodamine B	31	Water	514	110	190	1.60×10^{-131}
ICG	0.266	Water	820	0.96	0.77	4.72×10^{-4}
ICG	1.14	Blood	830	1.01	0.78	1.91×10^{-3}
Type II NIR quantum dots	13	PBS	840	1.05	0.78	2.09×10^{-2}
SWNT	0.1	PBS	1042	0.889	0.12	3.65×10^{-4}

PBS, phosphate-buffered saline
[a] Adapted from Barone and coauthors.[22]
[b] Calculated based on d = 1 cm and an average μ.

In addition to absorption, scattering also attenuates the fluorescent signal from optical sensors (**Figure 2C**).[44] The optical penetration depth in the tissue depends both on absorption and scattering: $\delta = (3\mu_a(\mu_a + \mu_S'))^{-1/2}$, where μ_a is the absorption coefficient and is the reduced scattering coefficient. The scattering coefficient varies with the wavelength: $\mu_S' \sim \lambda^{-w}$, where w is determined by the size and concentration of scatters and thus varies with tissue types.[44,45] Because of the inverse dependence of tissue scattering on the wavelength, long-wavelength NIR fluorophores could have a higher penetration depth in tissues than short-wavelength traditional visible fluorophores.

Experimental and simulation modeling studies of the effect of tissue scattering on the tissue penetration depth showed that the maximum penetration depth can be obtained at the wavelength range 1000–1400 nm, called the second NIR widow (NIR II).[44–47] Single-walled carbon nanotubes emit fluorescence within the NIR II, whereas most commercially available NIR fluorophores emit fluorescence in the NIR I (700 to 900 nm), including indocyanine green (ICG) and NIR fluorescent quantum dots.[44,48] The lower scattering and autofluorescence in the NIR II may compensate for higher absorption in NIR II (mostly due to water) than NIR I and make NIR II-emitting SWNTs outperform conventional NIR I-emitting fluorophores for *in vivo* applications (**Figure 2**).[44] Welsher and coauthors[44] studied the effect of tissue absorption and scattering on NIR I (ICG) and NIR II (SWNT) fluorophores in tissue phantoms (**Figure 3**).[49] This study shows a more pronounced loss of signal clarity as well as feature contrast and integrity in NIR I (ICG) than NIR II (SWNT; **Figure 3A** and **3B**), confirming the inverse wavelength dependence of the scattering effect.[49] The intensity profile as a function of tissue depth shows a similar attenuation in the fluorescence intensity at NIR I (ICG) and NIR II (SWNT), attributed to the combined absorbance and scattering effects (**Figure 3C**). An additional benefit of SWNTs (NIR II fluorophores) over traditional NIR I fluorophores includes a lower autofluorescence in the NIR II region, resulting from a larger Stokes shift between excitation and emission, which can be larger than 300 nm, and the longer excitation and emission wavelengths (because autofluorescence is mostly in the visible wavelength region).[44] **Figure 3D** shows a dynamic contrast-enhanced image with SWNTs through principal component analysis (left)[44] and NIR fluorescence image (right) of mice.[50]

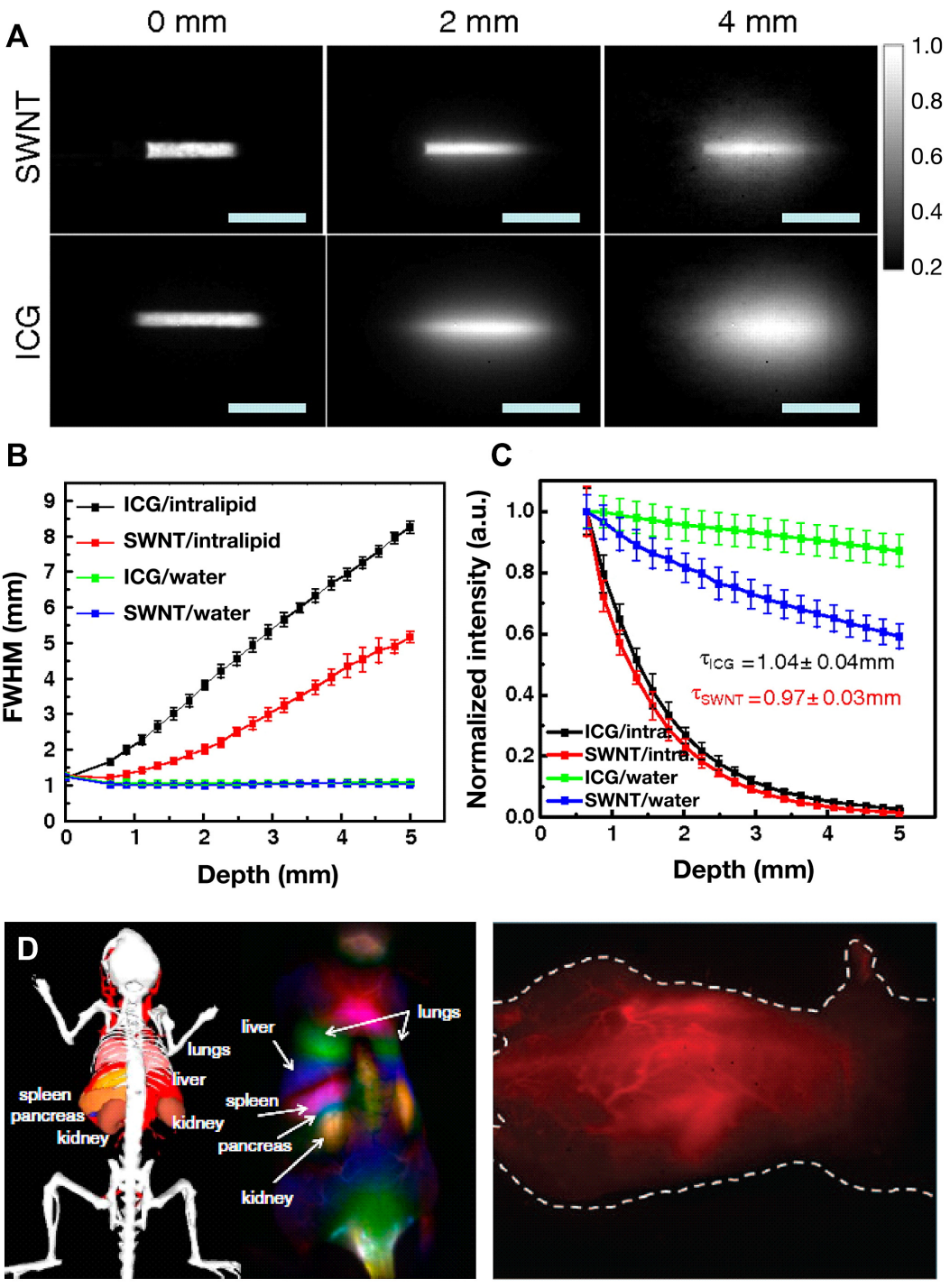

Figure 3. Optical penetration depth of NIR II-emitting SWNTs and NIR-I-emitting ICG in tissue phantoms. **(A)** Fluorescence images of capillaries filled with SWNTs (NIR II) and ICG (NIR I) at the depth of 0, 3, and 5 mm in Intralipid® excited at 785 nm. The fluorescence at NIR II (SWNT) shows a less loss of signal clarity and feature contrast and integrity (due to less scattering) than the fluorescence at NIR I (ICG) in the tissue phantom. Scale bars, 1.5 cm. **(B)** Feature width of SWNT and ICG capillary images as a function of depth in the tissue phantom, showing a more significant feature loss of NIR I-emitting ICG than NIR II-emitting SWNT. Control experiments done in water show no change in feature size for both ICG and SWNT. Error bars are derived from the uncertainty in the fitting of feature width. **(C)** Normalized intensity loss of ICG and SWNT as a function of depth in the tissue phantom (Intralipid) and water. Despite the higher absorption of water in NIR II, the decay of signal of ICG and SWNTs in the tissue phantom is similar, with the exponential decay depths of 1.04 ± 0.04 and 0.97 ± 0.03 mm, respectively. **(D)** Dynamic contrast-enhanced image with SWNTs through principal component analysis (left) and NIR fluorescence image (right) of mice. Reprinted with permission from *Proceedings of the National Academy of Sciences*[44] and *Nature Nanotechnology*.[50] FWHM, full width at half maximum.

The photostability of fluorophores determines the lifetime of optical sensors. Assuming the maximum tolerable error of viable *in vivo* glucose sensors of 20% for clinical applications,[5] a simple calculation from the attenuation factor of $e^{-k\tau}$ in the fluorescent signal intensity I_S estimates the lifetime τ of optical sensors as $\tau = -\ln(0.8/k)$. **Table 2** shows the estimated sensor lifetime calculated with literature values of the photobleaching rate constant k. Organic fluorophores are expected to have short lifetimes mostly because of a rapid photobleaching. Single-walled carbon nanotubes are the only known NIR fluorescent probe with no photobleaching threshold, ideal for long-term sensing applications.[51,52]

Table 2.
Photobleaching and Sensor Lifetime of Common Organic and Nanoparticle Fluorescent Probes[a]

Fluorescent probes	Photobleaching rate constant (h^{-1})	Fluence (mW/cm^2)	Irradiated sensor lifetime[b]
Infrared dye 78-CA	250.9	600	3.2 s
Cy5	20.5	600	39.1 s
ICG	0.0412	28	5.4 h
Type II NIR quantum dots	0.0827	600	2.7 h
SWNT	0	1.0×10^6	∞

[a] Adapted from Barone and coauthors.[22]
[b] Estimated sensor lifetime calculated from $\tau = -\ln(0.8/k)$.

Selective Modulation of Single-Walled Carbon Nanotube Fluorescence

The fluorescence of SWNTs is highly responsive to the local physical and chemical environment (e.g., local dielectric environment), making SWNTs a unique nanoscale optical sensing platform.[53–55] **Figure 4** shows five representative mechanisms for selective modulation of SWNT fluorescence.[35] Adsorption of a redox-active analyte to the nanotube surface can shift the nanotube Fermi level, inducing bleaching of the absorption transition and associated excitonic loss (mechanism 1, **Figure 4A**).[29,56] Examples of this mechanism include the binding of hydrogen peroxide and several other redox-active molecules and pH effects.[39,40,57] Secondly, exciton quenching through the nonradiative excited-electron transfer from nanotubes to the analyte adsorbed on the nanotubes can quench SWNT fluorescence (mechanism 2, **Figure 4B**).[32,33] Additionally, changes of the solvent environment lead to solvatochromic shift (mechanism 3, **Figure 4C**).[58] An example of this mechanism is the ion-induced conformational change of deoxyribonucleic-acid -encapsulated SWNTs.[59,60] Engineering polymer-wrapped nanotube complexes can also impart steric selectivity to the mechanism 3 (mechanism 4, **Figure 4D**). Another strategy for engineering selectivity is to conjugate an analyte-specific switchable polymer to the nanotubes (mechanism 5, **Figure 4E**).[35] An example is SWNT complexes wrapped by a polyvinyl alcohol (PVA) derivative functionalized with glucose-binding protein for glucose detection.[31] In reality, the modulation of SWNT fluorescence is often resulted from the combination of these mechanisms.

Single-Walled Carbon Nanotube-Based Near-Infrared Optical Glucose Sensors

We have demonstrated a proof-of-concept for modulating the NIR fluorescence of SWNTs in response to glucose and developed prototype SWNT-based glucose sensors.[29,30] A central challenge in designing SWNT-based sensors is to engineer the nanotube interface to be selective to glucose and effectively modulate SWNT fluorescence, while maintaining the colloidal stability of SWNT complexes. Because direct covalent functionalization of the surface of SWNTs disrupts SWNT fluorescent emission, noncovalent functionalization is required. Here we describe two SWNT-based glucose sensors: glucose-binding-protein-based and BA-based SWNT optical glucose sensors. Our earlier sensors have been reviewed previously.[7]

Glucose Binding Protein-Based Single-Walled Carbon Nanotube Glucose Sensors

Glucose-binding protein is a periplasmic-binding protein with high affinity for glucose that changes its conformation upon binding of glucose (from the open to the closed form; **Figure 5**).[61] We developed a GBP-based SWNT glucose

sensor by constructing PVA–GBP conjugates that wrap the nanotube (**Figure 5A**).[31] The GBP mechanically actuates the SWNT complex, resulting in reversible exciton quenching in response to glucose. The calibration curve shows the increase in fluorescence quenching with increasing glucose concentrations (**Figure 5B**). Furthermore, no response to glucose is observed for the same SWNT construct without GBP, which confirms the quenching mechanism (**Figure 5C**). The observed fluorescence quenching is selective to glucose, when compared with two other saccharides, with fructose and mannose showing a response of 40% and 20%, respectively, of the response to glucose at 10 mM (**Figure 5D**). As an illustration of a potential application, the GBP-based SWNT sensor solution is loaded into a dialysis capillary (10,000 molecular weight cut-off) to allow glucose to diffuse across the membrane while retaining the SWNT (**Figure 5E**). Cycling of the glucose level also shows a rapid and reversible change in SWNT fluorescence (**Figure 5F**).

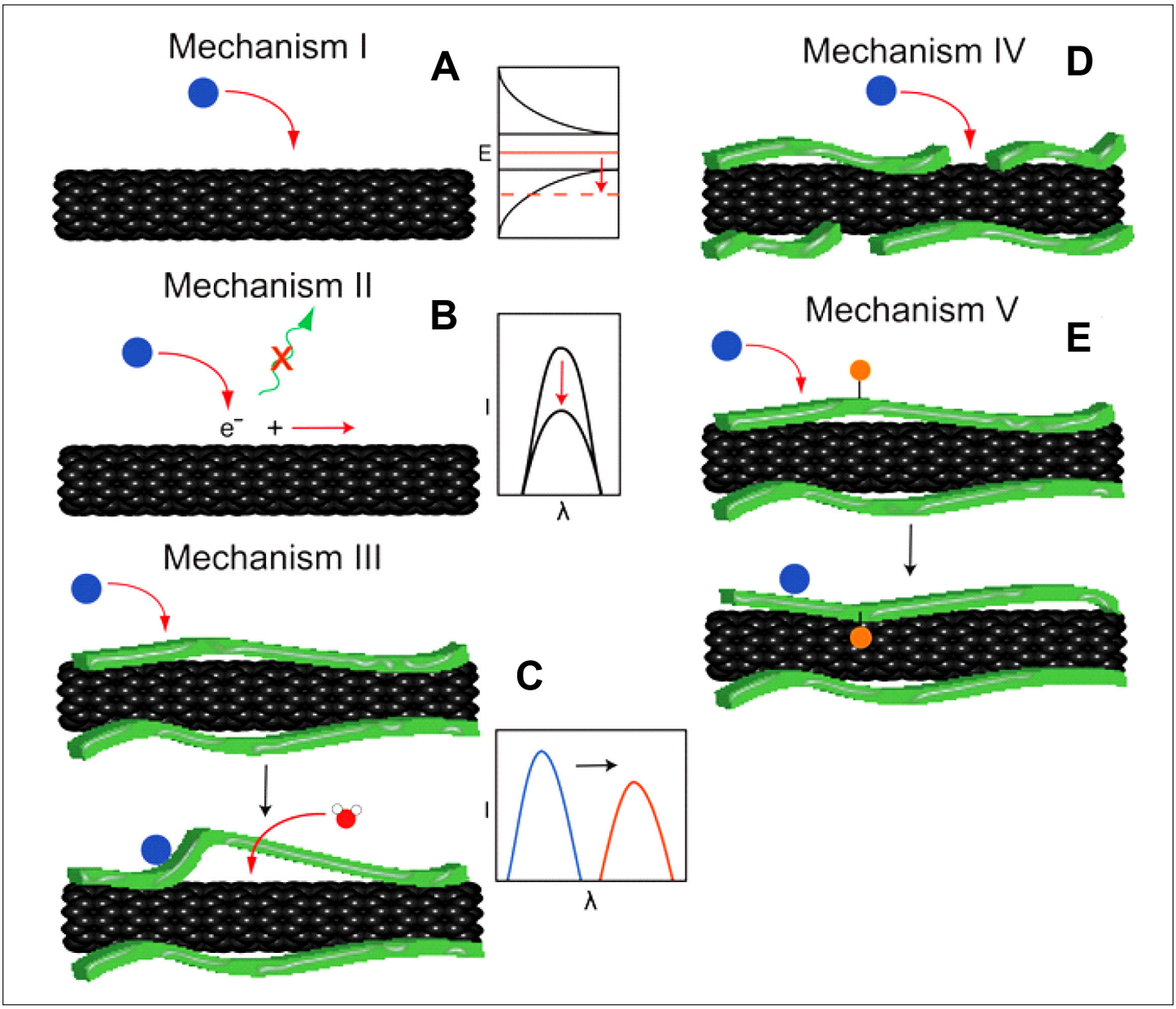

Figure 4. Representative mechanisms of SWNT fluorescence modulation. **(A)** Mechanism I, bleaching of the absorption transition induced by the shift of the Fermi level through the adsorption of redox-active analytes to the nanotube surface. **(B)** Mechanism II, fluorescence quenching resulted from nonradiative excited-electron transfer from nanotubes to the analyte adsorbed on the nanotubes induced by analyte binding. **(C)** Mechanism III, solvatochromic shifting resulting from the perturbation of SWNT-bound polymer. **(D)** Mechanism IV, selective analyte binding mediated by engineered polymer wrapping. **(E)** Mechanism V, analyte-activated polymer switching resulting in intensity and/or wavelength modulation. Reprinted with permission from *Proceedings of the National Academy of Sciences*.[35]

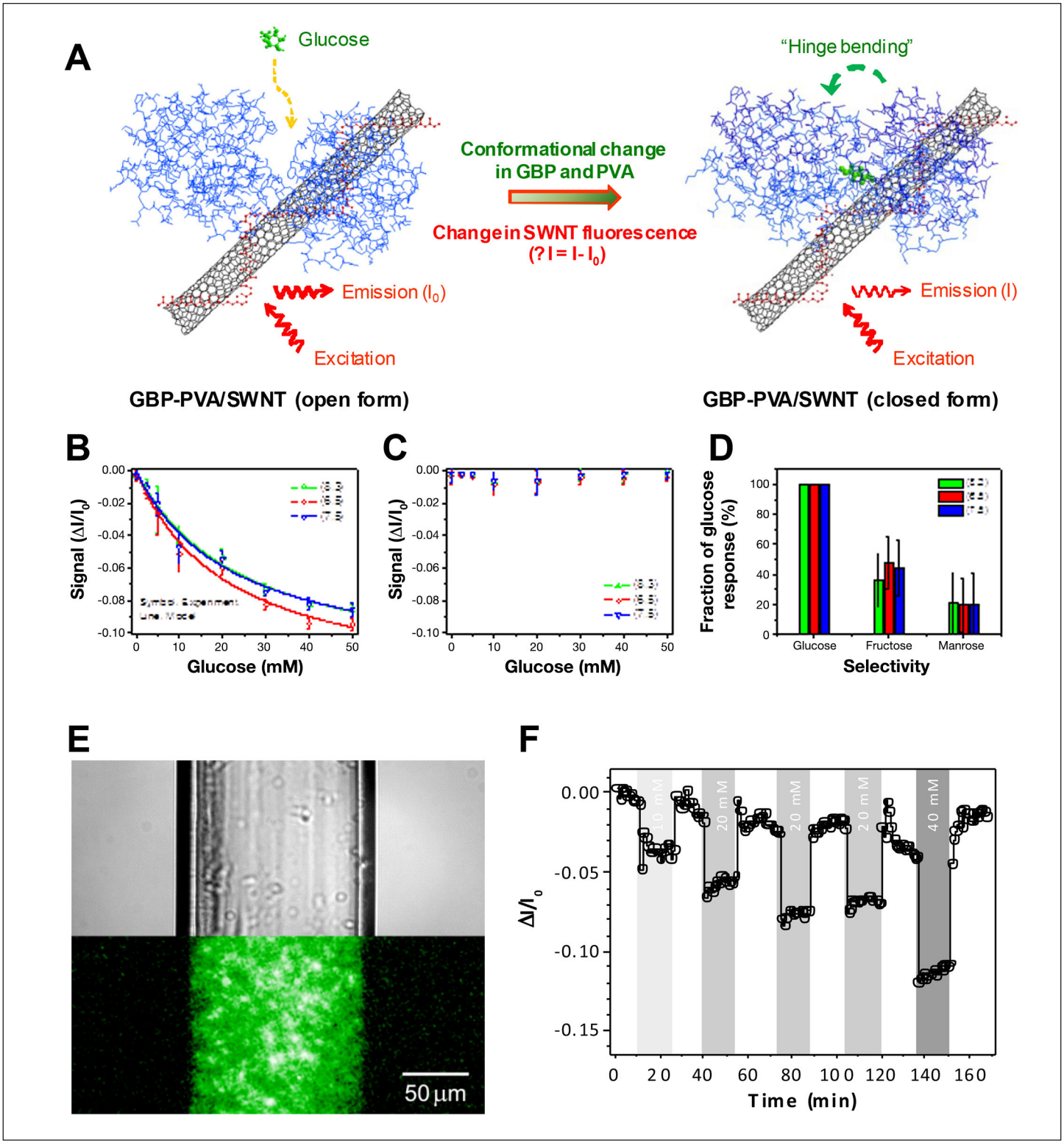

Figure 5. Glucose binding protein-based SWNT optical glucose sensors. **(A)** Schematic of the glucose recognition of the GBP–PVA/SWNT sensor. The difference in the angle between the two structural domains is the maximum of 36°, which arises from torsion angle changes in a three-segment hinge. **(B)** Calibration curve for GBP–PVA/SWNTs: steady-state responses of the fluorescent intensity of three different types of nanotubes to varying concentrations of glucose. **(C)** Histogram showing the selectivity of GBP–cationic-modified PVA/SWNTs over two other saccharides at 10 mM. **(D)** Optical and NIR fluorescent images of a 200 μm microdialysis capillary that encapsulates GBP–PVA/SWNTs. **(E)** Rapid and reversible response of GBP–PVA/SWNTs in the microdialysis capillary upon cyclic exposure to glucose. The gray-colored region indicates the presence of glucose. Reprinted with permission from *Angewandte Chemie International Edition*.[30]

Boronic-Acid-Based Single-Walled Carbon Nanotube Glucose Sensors

Boronic acids are an excellent molecular receptor for glucose.[62,63] The reversible complexation of glucose with aromatic BAs produces a stable boronate anion, changing the electronic properties of the BAs.[64–67] This alternation in the electronic properties of aromatic BAs upon binding of glucose has been a basic scheme for various BA-based glucose-sensing approaches.[63–66,68–70] It was hypothesized that the complexation of glucose with aromatic BAs conjugated on the surface of SWNTs could modulate the SWNT fluorescence signal in response to binding of glucose (**Figure 6**).[32] To test this concept and identify BAs that can be exploited as a molecular receptor for glucose in SWNT-based sensing systems, we screened the fluorescence spectral response of sodium cholate (SC)-suspended SWNTs (SC/SWNTs) against 30 BAs and the subsequent spectral change of the 30 BA–SWNT complexes in response to glucose.[32] The screening identifies 4-chlorophenylboronic acid (**Figure 6B**) and 4-cyanophenylboronic acid (**Figure 6C**), which uniquely show a reversible wavelength shift and a turn-on fluorescence response when complexed with SWNTs upon glucose binding. **Figure 6D** shows the fluorescence spectra of the quenched BA–SWNT complex of 4-cyanophenylboronic acid upon stepwise introduction of glucose: the BA–SWNT complex recovers the quenched fluorescence and the red-shifted emission wavelength with glucose concentration. **Figure 6E** shows the fluorescence intensity (left) and the emission wavelength (right) of (6,5) nanotubes as a function of glucose concentration: the BA–SWNT complexes respond to glucose in a physiologically important range of 0 to 30 mM.

This "turn-on" sensing scheme that uses the reversible fluorescence quenching and wavelength shift of the BA–SWNT complex has a potential to be applied to develop a highly stable and sensitive NIR optical glucose sensor. However, the current form of the BA-based SWNT sensors requires surfactant in the nanotube sensor solution to disperse the nanotubes in aqueous solutions.

Polymer complexes that can wrap SWNTs and disperse them in aqueous solutions and contain BA receptors to specifically detect not only glucose, but also other saccharides are thus under active research, including BA-conjugated polyethylene glycol-based polymer complexes.[71] In this work, we demonstrated both functions using a homologous series of seven phenyl BAs conjugated to a polyethylene glycol, eight-member, branched polymer (PPEG8) that allows for aqueous dispersion of SWNT and quenching of the NIR fluorescence in response to saccharide binding. We compared the 2-carboxyphenylboronic acid (CPBA), 3CPBA, 4CPBA, N-(4-Phenylboronic)succinamic acid, 5-Bromo-3-carboxy, 3-Carboxy-5-fluoro, and 3-carboxy-5-nitro, demonstrating a clear link between SWNT photoluminescence quantum yield and BA structure (**Figure 7**). Saccharide recognition using the NIR photoluminescence of SWNT is demonstrated, including selectivity toward pentoses such as arabinose, ribose, and xylose to the exclusion of the expected fructose (**Figure 8**). This study is the first to conclusively link molecular structure of an adsorbed phase to SWNT optical properties and modulation in a systematic manner.

Opportunities and Challenges for *In Vivo* Continuous Glucose Monitoring

Testing *in vivo* responses of the SWNT glucose sensors is critical for their clinical applications. A challenge is to improve the sensitivity, selectivity, and lifetime of the sensors in physiologically relevant conditions, including varying oxygen levels, pH, temperature, and potential interferents. An approach to achieve this is to use an internal reference by using two or more different types of SWNTs that emit fluorescence at different wavelengths for sensors and references, respectively. Another task to consider for *in vivo* applications is to construct microscale structures that encapsulate SWNT-based sensors. For *in vivo* sensing applications, the direct injection of nanoscale water-soluble SWNT sensors would not be practical, because the nanoscale SWNT sensors can circulate and distribute through the body;[44] instead, microscale glucose-responsive structure that are small enough to be injected or implemented in the body yet large enough to remain at the implantation site for a long period of time would be required for stable *in vivo* sensing.[72,73] Because the SWNT sensor is in aqueous suspension, the final sensor architecture is flexible, including dialysis capillary (**Figure 5E**)[29,31] and hydrogel microparticles that encapsulate SWNT glucose sensors (~100 μm in diameter).[72,73]

Another challenge is that sensors implanted in the body often fail because of biofouling of the sensor surface, inflammation, and fibrosis-induced vessel regression at the implantation site.[74–78] An approach to reduce the problems

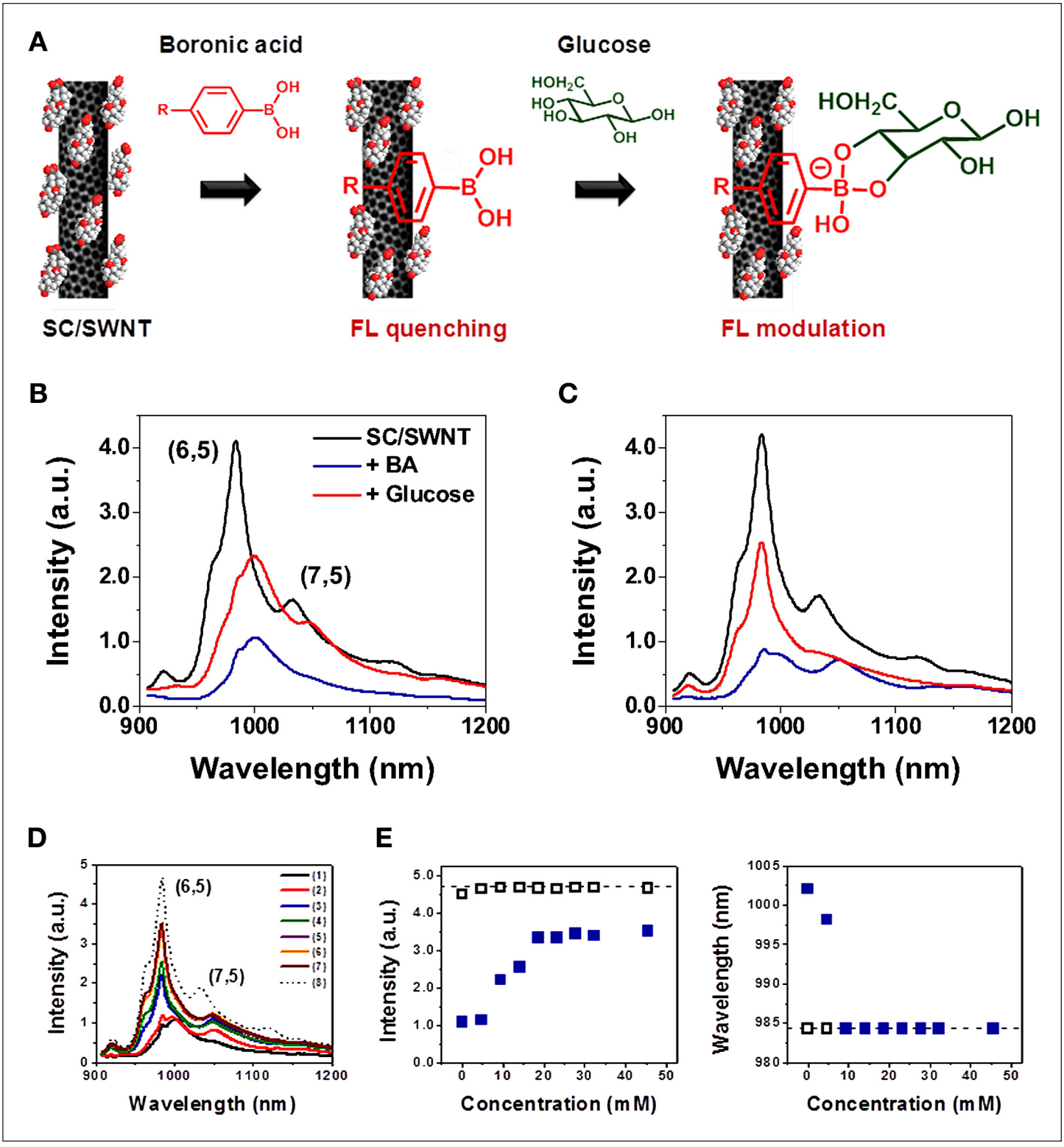

Figure 6. Reversible fluorescence quenching of BA–SWNT complexes for glucose detection. **(A)** Schematic illustration of the reaction of BAs with SC-suspended SWNTs (SC/SWNTs) and the fluorescence spectral response of the BA–SWNT complex to glucose. **(B),(C)** Fluorescence spectra that compare the original spectrum of SC/SWNTs (black), the spectrum after adding 50 mM BAs to SC/SWNT solutions (blue), and the spectrum after adding 50 mM glucose to the BA-SWNT complex solutions (red). The BA–SWNT complexes were prepared with **(B)** 4-chlorophenylboronic acid and **(C)** 4-cyanophenylboronic acid. Reprinted with permission *ACS Nano*.[32] FL, fluorescence.

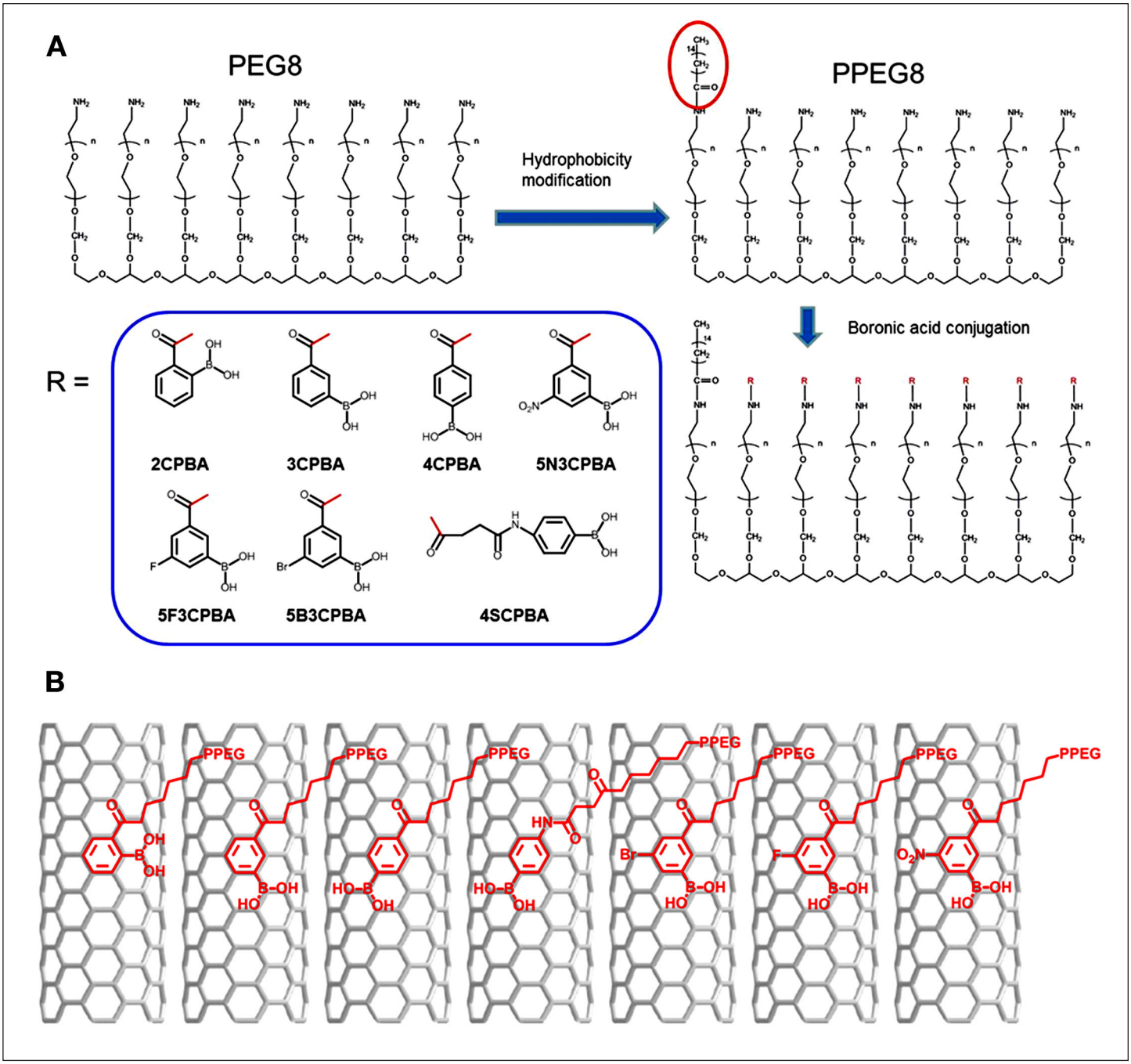

Figure 7. (A) Synthesis scheme of a series of phenylboronic acid conjugated amphiphilic polyethylene glycol polymers presents two steps, including hydrophobicity modification of PEG8 and BA conjugation. **(B)** Proposed wrapping geometry of different phenylboronic acids on a SWNT (from left to right: 2CPBA–PPEG8, 3CPBA–PPEG8, 4CPBA–PPEG8, N-(4-Phenylboronic)succinamic acid–PPEG8, 5-Bromo-3-carboxy–PPEG8, 3-Carboxy-5-fluoro–PPEG8, and 3-Carboxy-5-fluoro, and 3-carboxy-5-nitro–PPEG8). The highest photoluminescence quantum yield were observed for *para*-substituted phenylboronic acid (4CPBA), much higher than *ortho* (2CPBA)- and *meta* (3CPBA)-substituted phenylboronic acid. Reprinted with permission from Journal of the *American Chemical Society*.[71]

is to coat the surface of the glucose-sensing structure (e.g., hydrogel microparticles encapsulating SWNT glucose sensors) with the antifouling coating and incorporate anti-inflammatory agents, such as dexamethasone (DX), and angiogenic factors, such as vascular endothelial growth factor (VEGF), into the glucose-sensing structure.[74–78] For instance, delivering VEGF-producing cells to the site of glucose sensor implantation using a tissue-interactive fibrin biohydrogel induced significant neovascularization and improved the glucose sensor function *in vivo*.[76] The surface coating

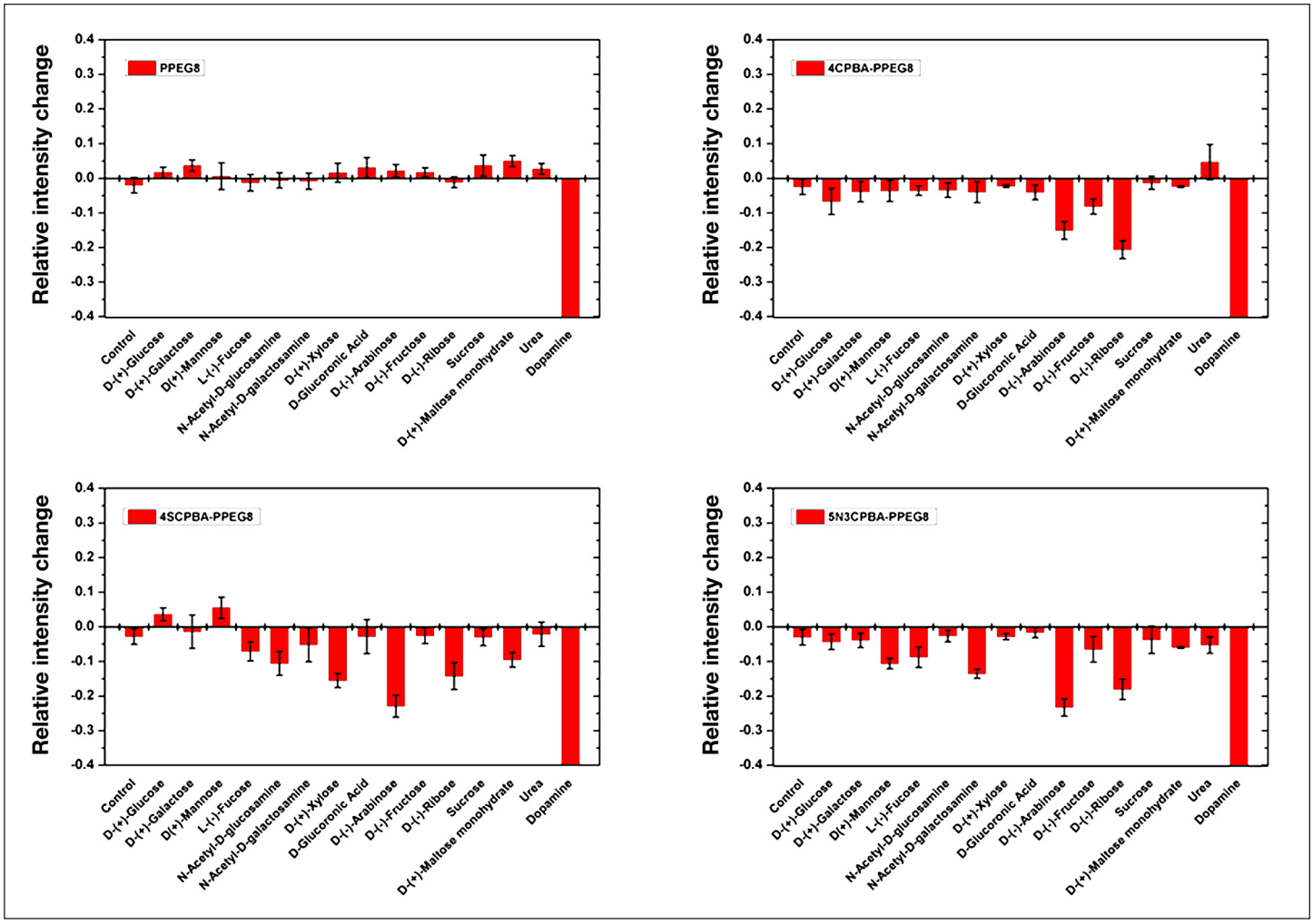

Figure 8. Response of saccharides in different phenylboronic acid–PPEG8 polymer dispersed SWNT solutions. All polymer-wrapped SWNT solutions were diluted using phosphate-buffered saline buffer to a final SWNT concentration of 2 mg/liter. The concentration of SWNT was determined using absorbance at 632 nm with c = 0.036 (mg/liter)$^{-1}$ cm^{-1}. All analytes were dissolved in water at 1 M concentration, and 2 μl analyte solutions were added to 200 μl SWNT, such that the final analyte concentration was 10 mM. The mixture solution was incubated for 1 h before the NIR fluorescence measurement. The intensity change is calculated based on the fluorescence of SWNT (9,4). Error bar is given by repeating three times for each measurement. Dopamine completely quenched fluorescence of SWNTs as a positive control. Reprinted with permission from Journal of the *American Chemical Society*.[71]

of hydrogels and microcapillaries with DX and VEGF and the release of DX and VEGF in the tissue reduced the biofouling and developed local environments favorable for long-term, reliable *in vivo* sensing.[74,79]

Testing the toxicity of SWNT sensors is an important issue for *in vivo* applications. Many studies have investigated the potential toxicity of carbon nanotubes to *in vitro* cell cultures and *in vivo* animal models and have shown various results, depending on the type and geometry of nanotubes, nanotube materials preparation, and surface functionalization.[27] Properly surface-functionalized carbon nanotubes have not induced obvious toxicity in cell culture experiments and *in vivo* studies,[80–83] whereas raw carbon has induced pulmonary toxicity and mechanical blockage of the upper airways in animal models.[84–88] Long MWNTs introduced into the abdominal cavity of mice also developed asbestos-like, length-dependent pathogenicity, including inflammation and formation of granulomas.[88] For the proposed SWNT-based *in vivo* glucose sensing, the SWNT sensor-encapsulating microstructures, such as hydrogel microparticles and microcapillaries, provide another protective layer (i.e., biocompatible hydrogels) other than biocompatible functionalization layers on SWNTs, which reduce the potential toxicity resulting from the direct contact of SWNTs with biological entities and the needle-like shape of SWNTs.[88] Considering the growing interest and use of SWNTs for biomedical application, further investigations are required to fully address the SWNT toxicology.[27,88]

Conclusions

SWNT-based NIR optical glucose sensors with their extraordinary NIR, nonphotobleaching fluorescence have a great potential for long-term *in vivo* CGM. A key challenge in designing SWNT-based glucose sensors is to identify and engineer molecular receptors for glucose that will work effectively in a SWNT sensing system and to understand how to effectively transfer glucose-binding events into the modulation of SWNT fluorescence to achieve the selectivity, sensitivity, and dynamic range of the sensors for *in vivo* glucose monitoring. Advancement of this technology also requires simultaneous research efforts toward translating the laboratory development of SWNT-based NIR optical glucose sensors into *in vivo* glucose sensing for practical clinical uses. The ability to sense glucose with nanoscale SWNT-based NIR optical sensors would also allow for new ways to answer important biological questions regarding glucose metabolism. The emerging technology of SWNT-based NIR optical glucose sensors can also be extended to various *in vivo* health monitoring systems.

Funding:

This work is funded by a grant from Sanofi-Aventis.

References:

1. World Health Organization. Diabetes: fact sheet N°312. http://www.who.int/mediacentre/factsheets/fs312/en.
2. Centers for Disease Control and Prevention. National diabetes fact sheet: national estimates and general information on diabetes and prediabetes in the United States, 2011. Atlanta: U.S. Department of Health and Human Services, Centers for Disease Control and Prevention; 2011. http://www.cdc.gov/diabetes/pubs/pdf/ndfs_2011.pdf.
3. The Diabetes Control and Complications Trial Research Group. The effect of intensive treatment of diabetes on the development and progression of long-term complications in insulin-dependent diabetes mellitus. N Engl J Med. 1993;329(14):977–86.
4. UK Prospective Diabetes Study (UKPDS). Intensive blood-glucose control with sulphonylureas or insulin compared with conventional treatment and risk of complications in patients with type 2 diabetes (UKPDS 33). Lancet. 1998;352(9131):837–53.
5. Heller A. Implanted electrochemical glucose sensors for the management of diabetes. Annu Rev Biomed Eng. 1999;1:153–75.
6. Zimmet P, Alberti KG, Shaw J. Global and societal implications of the diabetes epidemic. Nature. 2001;414(6865):782–7.
7. Barone PW, Strano MS. Single walled carbon nanotubes as reporters for the optical detection of glucose. J Diabetes Sci Technol. 2009;3(2):242–52.
8. Burge MR, Mitchell S, Sawyer A, Schade DS. Continuous glucose monitoring: the future of diabetes management. Diabetes Spectr. 2008;21(2):112–9.
9. Hermanides J, Phillip M, DeVries JH. Current application of continuous glucose monitoring in the treatment of diabetes: pros and cons. Diabetes Care. 2011;34 Suppl 2:S197–201.
10. Joubert M, Reznik Y. Personal continuous glucose monitoring (CGM) in diabetes management: review of the literature and implementation for practical use. Diabetes Res Clin Pract. 2012;96(3):294–305.
11. Wickramasinghe Y, Yang Y, Spencer SA. Current problems and potential techniques in *in vivo* glucose monitoring. J Fluoresc. 2004;14(5):513–20.
12. Moschou EA, Sharma BV, Deo SK, Daunert S. Fluorescence glucose detection: Advances toward the ideal *in vivo* biosensor. J Fluoresc. 2004;14(5):535–47.
13. Kondepati VR, Heise HM. Recent progress in analytical instrumentation for glycemic control in diabetic and critically ill patients. Anal Bioanal Chem. 2007;388(3):545–63.
14. Ferrante do Amaral CE, Wolf B. Current development in non-invasive glucose monitoring. Med Eng Phys. 2008;30(5):541–9.
15. Cash KJ, Clark HA. Nanosensors and nanomaterials for monitoring glucose in diabetes. Trends Mol Med. 2010;16(12):584–93.
16. Steiner MS, Duerkop A, Wolfbeis OS. Optical methods for sensing glucose. Chem Soc Rev. 2011;40(9):4805–39.
17. Gandhi GY, Kovalaske M, Kudva Y, Walsh K, Elamin MB, Beers M, Coyle C, Goalen M, Murad MS, Erwin PJ, Corpus J, Montori VM, Murad MH. Efficacy of continuous glucose monitoring in improving glycemic control and reducing hypoglycemia: a systematic review and meta-analysis of randomized trials. J Diabetes Sci Technol. 2011;5(4):952–65.
18. Ciudin A, Hernandez C, Simo R. Non-invasive methods of glucose measurement: Current status and future perspectives. Curr Diabetes Rev. 2012;8(1):48–54.
19. Wang J. Electrochemical glucose biosensors. Chem Rev. 2008;108(2):814–25.
20. Vaddiraju S, Tomazos I, Burgess DJ, Jain FC, Papadimitrakopoulos F. Emerging synergy between nanotechnology and implantable biosensors: a review. Biosens Bioelectron. 2010;25(7):1553–65.

21. Wilson GS, Gifford R. Biosensors for real-time *in vivo* measurements. Biosens Bioelectron. 2005;20(12):2388–403.
22. Barone PW, Parker RS, Strano MS. *In vivo* fluorescence detection of glucose using a single-walled carbon nanotube optical sensor: design, fluorophore properties, advantages, and disadvantages. Anal Chem. 2005;77(23):7556–62.
23. Pickup JC, Hussain F, Evans ND, Rolinski OJ, Birch DJ. Fluorescence-based glucose sensors. Biosens Bioelectron. 2005;20(12):2555–65.
24. Zanon M, Sparacino G, Facchinetti A, Riz M, Talary MS, Suri RE, Caduff A, Cobelli C. Non-invasive continuous glucose monitoring: improved accuracy of point and trend estimates of the multisensor system. Med Biol Eng Comput. 2012;50(10):1047–57.
25. Tura A, Maran A, Pacini G. Non-invasive glucose monitoring: Assessment of technologies and devices according to quantitative criteria. Diabetes Res Clin Pract. 2007;77(1):16–40.
26. Wray S, Cope M, Delpy DT, Wyatt JS, Reynolds EO. Characterization of the near infrared absorption spectra of cytochrome aa3 and haemoglobin for the non-invasive monitoring of cerebral oxygenation. Biochim Biophys Acta. 1988;933(1):184–92.
27. Liu Z, Tabakman S, Welsher K, Dai H. Carbon nanotubes in biology and medicine: *in vitro* and *in vivo* detection, imaging and drug delivery. Nano Res. 2009;2(2):85–120.
28. Boghossian AA, Zhang J, Barone PW, Reuel NF, Kim JH, Heller DA, Ahn JH, Hilmer AJ, Rwei A, Arkalgud JR, Zhang CT, Strano MS. Near-infrared fluorescent sensors based on single-walled carbon nanotubes for life sciences applications. ChemSusChem. 2011;4(7):848–63.
29. Barone PW, Baik S, Heller DA, Strano MS. Near-infrared optical sensors based on single-walled carbon nanotubes. Nat Mater. 2005;4(1):86–92.
30. Barone PW, Strano MS. Reversible control of carbon nanotube aggregation for a glucose affinity sensor. Angew Chem Int Ed Engl. 2006;45(48):8138–41.
31. Yoon H, Ahn JH, Barone PW, Yum K, Sharma R, Boghossian AA, Han JH, Strano MS. Periplasmic binding proteins as optical modulators of single-walled carbon nanotube fluorescence: amplifying a nanoscale actuator. Angew Chem Int Ed Engl. 2011;50(8):1828–31.
32. Yum K, Ahn JH, McNicholas TP, Barone PW, Mu B, Kim JH, Jain RM, Strano MS. Boronic acid library for selective, reversible near-infrared fluorescence quenching of surfactant suspended single-walled carbon nanotubes in response to glucose. ACS Nano. 2012;6(1):819–30.
33. Satishkumar BC, Brown LO, Gao Y, Wang CC, Wang HL, Doorn SK. Reversible fluorescence quenching in carbon nanotubes for biomolecular sensing. Nat Nanotechnol. 2007;2(9):560–4.
34. Kim JH, Heller DA, Jin H, Barone PW, Song C, Zhang J, Trudel LJ, Wogan GN, Tannenbaum SR, Strano MS. The rational design of nitric oxide selectivity in single-walled carbon nanotube near-infrared fluorescence sensors for biological detection. Nat Chem. 2009;1(6):473–81.
35. Heller DA, Pratt GW, Zhang J, Nair N, Hansborough AJ, Boghossian AA, Reuel NF, Barone PW, Strano MS. Peptide secondary structure modulates single-walled carbon nanotube fluorescence as a chaperone sensor for nitroaromatics. Proc Natl Acad Sci U S A. 2011;108(21):8544–9.
36. Ahn JH, Kim JH, Reuel NF, Barone PW, Boghossian AA, Zhang J, Yoon H, Chang AC, Hilmer AJ, Strano MS. Label-free, single protein detection on a near-infrared fluorescent single-walled carbon nanotube/protein microarray fabricated by cell-free synthesis. Nano Lett. 2011;11(7):2743–52.
37. Reuel NF, Ahn JH, Kim JH, Zhang J, Boghossian AA, Mahal LK, Strano MS. Transduction of glycan-lectin binding using near-infrared fluorescent single-walled carbon nanotubes for glycan profiling. J Am Chem Soc. 2011;133(44):17923–33.
38. Cognet L, Tsyboulski DA, Rocha JD, Doyle CD, Tour JM, Weisman RB. Stepwise quenching of exciton fluorescence in carbon nanotubes by single-molecule reactions. Science. 2007;316(5830):1465–8.
39. Jin H, Heller DA, Kim JH, Strano MS. Stochastic analysis of stepwise fluorescence quenching reactions on single-walled carbon nanotubes: single molecule sensors. Nano Lett. 2008;8(12):4299–304.
40. Heller DA, Jin H, Martinez BM, Patel D, Miller BM, Yeung TK, Jena PV, Höbartner C, Ha T, Silverman SK, Strano MS. Multimodal optical sensing and analyte specificity using single-walled carbon nanotubes. Nat Nanotechnol. 2009;4(2):114–20.
41. Bachilo SM, Strano MS, Kittrell C, Hauge RH, Smalley RE, Weisman RB. Structure-assigned optical spectra of single-walled carbon nanotubes. Science. 2002;298(5602):2361–6.
42. O'Connell MJ, Bachilo SM, Huffman CB, Moore VC, Strano MS, Haroz EH, Rialon KL, Boul PJ, Noon WH, Kittrell C, Ma J, Hauge RH, Weisman RB, Smalley RE. Band gap fluorescence from individual single-walled carbon nanotubes. Science. 2002;297(5581):593–6.
43. Hartschuh A, Pedrosa HN, Novotny L, Krauss TD. Simultaneous fluorescence and raman scattering from single carbon nanotubes. Science. 2003;301(5638):1354–6.
44. Welsher K, Sherlock SP, Dai H. Deep-tissue anatomical imaging of mice using carbon nanotube fluorophores in the second near-infrared window. Proc Natl Acad Sci U S A. 2011;108(22):8943–8.
45. Bashkatov AN, Genina EA, Kochubey VI, Tuchin VV. Optical properties of human skin, subcutaneous and mucous tissues in the wavelength range from 400 to 2000 nm. J Phys D. 2005;38(15):2543–55.
46. Troy TL, Thennadil SN. Optical properties of human skin in the near infrared wavelength range of 1000 to 2200 nm. J Biomed Opt. 2001;6(2):167–76.
47. Lim YT, Kim S, Nakayama A, Stott NE, Bawendi MG, Frangioni JV. Selection of quantum dot wavelengths for biomedical assays and imaging. Mol Imaging. 2003;2(1):50–64.
48. Michalet X, Pinaud FF, Bentolila LA, Tsay JM, Doose S, Li JJ, Sundaresan G, Wu AM, Gambhir SS, Weiss S. Quantum dots for live cells, *in vivo* imaging, and diagnostics. Science. 2005;307(5709):538–44.
49. Van Staveren HJ, Moes CJ, van Marie J, Prahl SA, van Gemert MJ. Light scattering in intralipid-10% in the wavelength range of 400-1100 nm. Appl Opt. 1991;30(31):4507–14.
50. Welsher K, Liu Z, Sherlock SP, Robinson JT, Chen Z, Daranciang D, Dai H. A route to brightly fluorescent carbon nanotubes for near-infrared imaging in mice. Nat Nanotechnol. 2009;4(11):773–80.

51. Cherukuri P, Bachilo SM, Litovsky SH, Weisman RB. Near-infrared fluorescence microscopy of single-walled carbon nanotubes in phagocytic cells. J Am Chem Soc. 2004;126(48):15638–9.
52. Heller DA, Baik S, Eurell TE, Strano MS. Single-walled carbon nanotube spectroscopy in live cells: towards long-term labels and optical sensors. Adv Mater. 2005;17(23):2793–9.
53. Strano MS, Moore VC, Miller MK, Allen MJ, Haroz EH, Kittrell C, Hauge RH, Smalley RE. The role of surfactant adsorption during ultrasonication in the dispersion of single-walled carbon nanotubes. J Nanosci Nanotechnol. 2003;3(1-2):81–6.
54. Walsh AG, Vamivakas AN, Yin Y, Cronin SB, Unlü MS, Goldberg BB, Swan AK. Screening of excitons in single, suspended carbon nanotubes. Nano Lett. 2007;7(6):1485–8.
55. Barone PW, Yoon H, Ortiz-García R, Zhang J, Ahn JH, Kim JH, Strano MS. Modulation of single-walled carbon nanotube photoluminescence by hydrogel swelling. ACS Nano. 2009;3(12):3869–77.
56. O' Connell MJ, Eibergen EE, Doorn SK. Chiral selectivity in the charge-transfer bleaching of single-walled carbon-nanotube spectra. Nat Mater. 2005;4(5):412–8.
57. Tu X, Pehrsson PE, Zhao W. Redox reaction of DNA-encased hipco carbon nanotubes with hydrogen peroxide: a near infrared optical sensitivity and kinetics study. J Phys Chem C. 2007;111(46):17227–31.
58. Choi JH, Strano MS. Solvatochromism in single-walled carbon nanotubes. Appl Phys Lett. 2007;90(22):223114.
59. Heller DA, Jeng ES, Yeung TK, Martinez BM, Moll AE, Gastala JB, Strano MS. Optical detection of DNA conformational polymorphism on single-walled carbon nanotubes. Science. 2006;311(5760):508–11.
60. Jin H, Jeng ES, Heller DA, Jena PV, Kirmse R, Langowski J, Strano MS. Divalent ion and thermally induced DNA conformational polymorphism on single-walled carbon nanotubes. Macromolecules. 2007;40(18):6731–9.
61. Dwyer MA, Hellinga HW. Periplasmic binding proteins: a versatile superfamily for protein engineering. Curr Opin Struct Biol. 2004;14(4):495–504.
62. James TD, Sandanayake KR, Shinkai S. Saccharide sensing with molecular receptors based on boronic acid. Angew Chem Int Ed. 1996;35:1910–22.
63. Mader HS, Wolfbeis OS. Boronic acid based probes for microdetermination of saccharides and glycosylated biomolecules. Microchim Acta. 2008;162:1–34.
64. Ori A, Shinkai S. Electrochemical detection of saccharides by the redox cycle of a chiral ferrocenylboronic acid derivative: a novel method for sugar sensing. J Chem Soc Chem Commun. 1995;17:1771–2.
65. Shoji E, Freund MS. Potentiometric saccharide detection based on the pk(a) changes of poly(aniline boronic acid). J Am Chem Soc. 2002;124(42):12486–93.
66. Takahashi S, Anzai J. Phenylboronic acid monolayer-modified electrodes sensitive to sugars. Langmuir. 2005;21(11):5102–7.
67. Cordes DB, Gamsey S, Singaram B. Fluorescent quantum dots with boronic acid substituted viologens to sense glucose in aqueous solution. Angew Chem Int Ed Engl. 2006;45(23):3829–32.
68. James TD, Sandanayake KR, Shinkai S. Chiral discrimination of monosaccharides using a fluorescent molecular sensor. Nature. 1995;374:345–7.
69. Fang H, Kaur G, Wang B. Progress in boronic acid-based fluorescent glucose sensors. J Fluoresc. 2004;14(5):481–9.
70. Edwards NY, Sager TW, McDevitt JT, Anslyn EV. Boronic acid based peptidic receptors for pattern-based saccharide sensing in neutral aqueous media, an application in real-life samples. J Am Chem Soc. 2007;129(44):13575–83.
71. Mu B, McNicholas TP, Zhang J, Hilmer AJ, Jin Z, Reuel NF, Kim JH, Yum K, Strano MS. A structure-function relationship for the optical modulation of phenyl boronic acid-grafted, polyethylene glycol-wrapped single-walled carbon nanotubes. J Am Chem Soc. 2012;134(42):17620–7.
72. Shibata H, Heo YJ, Okitsu T, Matsunaga Y, Kawanishi T, Takeuchi S. Injectable hydrogel microbeads for fluorescence-based *in vivo* continuous glucose monitoring. Proc Natl Acad Sci U S A. 2010;107(42):17894–8.
73. Heo YJ, Shibata H, Okitsu T, Kawanishi T, Takeuchi S. Long-term *in vivo* glucose monitoring using fluorescent hydrogel fibers. Proc Natl Acad Sci U S A. 2011;108(33):13399–403.
74. Sung J, Barone PW, Kong H, Strano MS. Sequential delivery of dexamethasone and vegf to control local tissue response for carbon nanotube fluorescence based micro-capillary implantable sensors. Biomaterials. 2009;30(4):622–31.
75. Klueh U, Dorsky DI, Kreutzer DL. Use of vascular endothelial cell growth factor gene transfer to enhance implantable sensor function *in vivo*. J Biomed Mater Res A. 2003;67(4):1072–86.
76. Klueh U, Dorsky DI, Kreutzer DL. Enhancement of implantable glucose sensor function *in vivo* using gene transfer-induced neovascularization. Biomaterials. 2005;26(10):1155–63.
77. Rebrin K, Fischer U, Hahn von Dorsche H, von Woetke T, Abel P, Brunstein E. Subcutaneous glucose monitoring by means of electrochemical sensors: fiction or reality? J Biomed Eng. 1992;14(1):33–40.
78. Abel PU, Von Woedtke T. Biosensors for *in vivo* glucose measurement: can we cross the experimental stage. Biosens Bioelectron. 2002;17(11-12):1059–70.
79. Norton LW, Tegnell E, Toporek SS, Reichert WM. *In vitro* characterization of vascular endothelial growth factor and dexamethasone releasing hydrogels for implantable probe coatings. Biomaterials. 2005;26(16):3285–97.
80. Shi Kam NW, Jessop TC, Wender PA, Dai H. Nanotube molecular transporters: internalization of carbon nanotube-protein conjugates into mammalian cells. J Am Chem Soc. 2004;126(22):6850–1.

81. Dumortier H, Lacotte S, Pastorin G, Marega R, Wu W, Bonifazi D, Briand JP, Prato M, Muller S, Bianco A. Functionalized carbon nanotubes are non-cytotoxic and preserve the functionality of primary immune cells. Nano Lett. 2006;6(7):1522–8.

82. Schipper ML, Nakayama-Ratchford N, Davis CR, Kam NW, Chu P, Liu Z, Sun X, Dai H, Gambhir SS. A pilot toxicology study of single-walled carbon nanotubes in a small sample of mice. Nat Nanotechnol. 2008;3(4):216–21.

83. Wu P, Chen X, Hu N, Tam UC, Blixt O, Zettl A, Bertozzi CR. Biocompatible carbon nanotubes generated by functionalization with glycodendrimers. Angew Chem Int Ed Engl. 2008;47(27):5022–5.

84. Lam CW, James JT, McCluskey R, Hunter RL. Pulmonary toxicity of single-wall carbon nanotubes in mice 7 and 90 days after intratracheal instillation. Toxicol Sci. 2004;77(1):126–34.

85. Warheit DB, Laurence BR, Reed KL, Roach DH, Reynolds GA, Webb TR. Comparative pulmonary toxicity assessment of single-wall carbon nanotubes in rats. Toxicol Sci. 2004;77(1):117–25.

86. Muller J, Huaux F, Moreau N, Misson P, Heilier JF, Delos M, Arras M, Fonseca A, Nagy JB, Lison D. Respiratory toxicity of multi-wall carbon nanotubes. Toxicol Appl Pharmacol. 2005;207(3):221–31.

87. Shvedova AA, Kisin ER, Mercer R, Murray AR, Johnson VJ, Potapovich AI, Tyurina YY, Gorelik O, Arepalli S, Schwegler-Berry D, Hubbs AF, Antonini J, Evans DE, Ku BK, Ramsey D, Maynard A, Kagan VE, Castranova V, Baron P. Unusual inflammatory and fibrogenic pulmonary responses to single-walled carbon nanotubes in mice. Am J Physiol Lung Cell Mol Physiol. 2005;289(5):L698–708.

88. Poland CA, Duffin R, Kinloch I, Maynard A, Wallace WA, Seaton A, Stone V, Brown S, Macnee W, Donaldson K. Carbon nanotubes introduced into the abdominal cavity of mice show asbestos-like pathogenicity in a pilot study. Nat Nanotechnol. 2008;3(7):423–8.